proceedings

MDPI

Proceedings

Boosted Kerr Black Hole in the Presence of Plasma †

Carlos A. Benavides-Gallego [1,*] and Ahmadjon Abdujabbarov [1,2,*]

[1] Center for Field Theory and Particle Physics and Department of Physics, Fudan University, Shanghai 200438, China
[2] Ulugh Beg Astronomical Institute, Astronomicheskaya 33, Tashkent 100052, Uzbekistan
* Correspondence: abgcarlos17@fudan.edu.cn (C.A.B.-G.); ahmadjon@fudan.edu.cn (A.A.)
† Presented at the Recent Progress in Relativistic Astrophysics, Shanghai, China, 6–8 May 2019.

Received: 25 July 2019; Accepted: 26 August 2019; Published: 4 September 2019

Abstract: In this work, we obtain the deflection angle for a boosted Kerr black hole in the weak field approximation using the optics in a curved spacetime developed by J. L. Synge in 1960. We study the behavior of light in the presence of plasma by considering different distributions: uniform plasma, singular isothermal sphere, non-singular isothermal gas sphere, and plasma in a galaxy cluster. We found that the dragging of the inertial system along with the boosted parameter Λ affect the value of the deflection angle. As an application, we studied the magnification for both uniform and singular isothermal distributions.

Keywords: optics in curved spacetimes; gravitational lensing; weak field limit; boosted Kerr metric; plasma distribuions; magnification

1. Introduction

The detection of gravitational waves from the coalescence of two black holes showed the formation of a rapidly rotating black hole boosted with linear velocity [1,2]. Furthermore, the possible observation of the electromagnetic counterpart from black hole merger could provide more information about angular and linear momentum in such systems [3,4]. In this sense, it is important to include the boost parameter into the Kerr black hole solution to investigate possibles effects on the gravitational field.

On the other hand, gravitational lensing has been used as a tool to test Einstein's theory of gravity and a lot of work has been done in this field by the scientific community. Starting from the work of Synge on optics in a curved spacetime [5], for example, it has been shown that the photon motion is affected by the presence of plasma [6–8]. Moreover, the effect of plasma around a compact objects on lensing effects has been studied in [9–13] and references there in. In the literature, there is also a lot of work devoted to the so-called black hole shadow [14–23] and references there in.

Recently, a solution of Einstein's vacuum field equations which describes a boosted Kerr black hole relative to an asymptotic Lorentz frame was obtained in Ref. [24]. This solution opens the possibility to study the weak gravitational lensing effect around a boosted Kerr black hole in the presence of plasma. Hence, in the present manuscript, we study the gravitational lensing effect around a boosted black hole by considering different plasma distributions. The paper is organized as follow. First, we briefly discuss the optics in curved spacetimes and describe the procedure to obtain the deflection angle in the weak field approximation following works of Ref. [6,8]. Then, we present the boosted Kerr metric in both non-rotating and slowly rotating cases. Next, following the previous discussion, we find the deflection angle and study its behavior in the presence of plasma, both for uniform and non-uniform distributions (singular isothermal sphere (**SIS**), non-singular isothermal sphere (**NSIS**), and the case of a plasma in a galaxy cluster (**PGC**).) Finally, as an application, we study the magnification for uniform and **SIS** plasma distributions.

Throughout the paper, we use geometrized units where $c = G = 1$ (with the execption of Section 2) and the convention in which Greek indices run from 0 to 3, while Latin indices run from 1 to 3. Finally, we want to point out that this work was presented as a talk at the meeting: *Progress in Relativistic Astrophysics* at Fudan University and it is based on the paper: "Gravitational lensing for a boosted Kerr black hole in the presence of plasma" published by the European physics journal C.

2. Optics in a Curved Space-Time

Our main goal is to study the effect of plasma on the gravitational lensing for a boosted Kerr black hole in the weak-field limit. For this reason, we consider a static spacetime metric which describes a weak gravitational field $g_{\mu\nu}$ and has the form [6,8]

$$g^{\alpha\beta} = \eta^{\alpha\beta} - h^{\alpha\beta} \quad \text{and} \quad g_{\alpha\beta} = \eta_{\alpha\beta} + h_{\alpha\beta}, \tag{1}$$

where $\eta_{\alpha\beta}$ is the Minkowski spacetime, $h_{\alpha,\beta}$ are small perturbation ($h_{\alpha\beta} \ll 1$) and $h_{\alpha\beta} \to 0$ for $x^{\alpha} \to \infty$ and $h^{\alpha\beta} = h_{\alpha\beta}$. The form of $g_{\mu\nu}$ in Equation (1), in the context of general relativity, means that the spacetime metric is nearly flat [25]. In this sense, our study is done far from the gravitational field of the source where gravity is "weak". Also, the assumption of a weak field, enable us to consider an approximation in the motion of photons: *the null approximation*.

Before studying the gravitational lensing for a boosted Ker black hole surrounded by plasma, it is necessary to obtain the equation of motion for photons in the presence of a gravitational field and include the plasma contribution into these equations. To do so, we follow the ideas of J.L. Synge [5] and the works of Bisnovatyi-Kogan et al. and V. S. Morozova et al. [6,8]. In reference [5], where the optics in a curved-spacetime was first developed, Synge starts by considering a *single infinity 3-spaces*. These *single infinity 3-spaces*, can be spacelike, null, or timelike and are called *waves* or *phase-waves* by the author (see Figure 1).

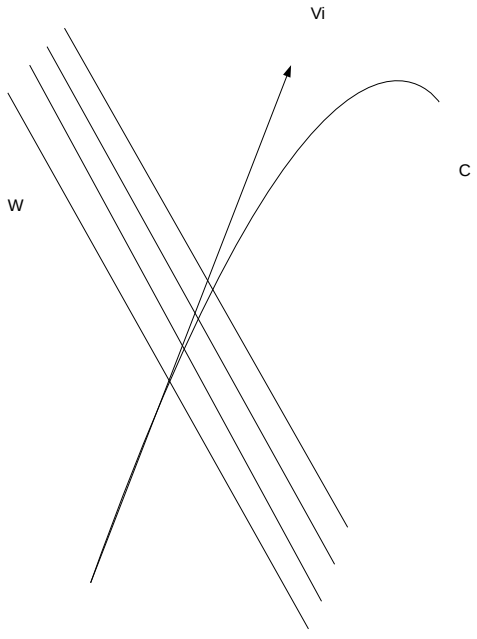

Figure 1. Phase-waves and observer C with 4-velocity V^{μ}.

Then, using this approach, he was able to obtain the frequency ω and speed u of the wave relative to the observer (later, the observer C will be the medium. This means that both the frequency and

velocity of the wave will be measured at the instantaneous rest frame of the plasma.), which are given by the relations [5]

$$p_\mu V^\mu = -\frac{\hbar\omega}{c} \tag{2}$$

and

$$\frac{c^2}{u^2} = 1 - \frac{p_\mu p^\mu}{(p_\nu V^\nu)^2}. \tag{3}$$

Here $\hbar$ is the Planck's constant and c is the speed of light. Equations (2) and (3) play an important roll in the optics theory developed by J.L. Synge. Hence, using the Hamiltonian formalism, he shows that the variational principle

$$\delta\left(\int p_\alpha dx^\alpha\right) = 0, \tag{4}$$

along with the condition

$$W(x^\alpha, p_\alpha) = \frac{1}{2}\left[g^{\alpha\beta}p_\alpha p_\beta - (n^2-1)\left(p_\alpha V^\alpha\right)^2\right] = 0 \tag{5}$$

leads to the following system of differential equations [5]

$$\frac{dx^\alpha}{d\lambda} = \frac{\partial W}{\partial p_\alpha} \quad \text{and} \quad \frac{dp_\alpha}{d\lambda} = -\frac{\partial W}{\partial x^\alpha}, \tag{6}$$

where the affine parameter λ changes along the light trajectory. Note that the scalar function $W(x_\alpha, p_\alpha)$ has been defined from the relationship between the phase velocity (The phase velocity is defined as the minimum value of

$$u'^2 = 1 + \frac{dx_\alpha dx^\alpha}{(V_\beta dx^\beta)^2},$$

where u' is the velocity of a fictitious particle riding on the wavefront relative to a time-like world-line C (intersecting the wave) of an observer with 4-velocity V^μ (see [5] for details).) u and the 4-vector of the photon momentum p^α (given by Equation (3)) so that the Hamiltonian formalism can be considered. Thus, Equation (6) describes the photons' trajectories in a gravitational field. Now, to include the effect of plasma in the equations of motion, G .S. Bisnovatyi-Kogan and O. Y. Tsupko consider a static inhomogeneous plasma with a refraction index n that depends on the space location x^i. Mathematically, this refraction index is given by [6,8]

$$n^2 = 1 - \frac{\omega_e^2}{[\omega(x^i)]^2} \quad \text{and} \quad \omega_e^2 = \frac{4\pi e^2 N(x^i)}{m} = K_e N(x^i), \tag{7}$$

where e and m are the electron charge and mass respectively, ω_e is the plasma frequency, and $N(x^i)$ is the electron concentration in an inhomogeneous plasma. The photon frequency $\omega(x^i)$ depends on the space coordinates x^1, x^2, x^3 due to gravitational redshift [8].

It is known that for a static medium in a static gravitational field, the photon energy can be expressed as [5,6,8]

$$p_\alpha V^\alpha = -\frac{1}{c}\hbar\omega(x^i) = p_0\sqrt{-g^{00}}. \tag{8}$$

Therefore, after using Equation (5) the function $W(x^\alpha, p_\alpha)$ reduces to

$$W(x^\alpha, p_\alpha) = \frac{1}{2}\left[g^{\alpha\beta}p_\alpha p_\beta + \frac{\omega_e^2\hbar^2}{c^2}\right], \tag{9}$$

The scalar function expressed in Equation (9) has been used in references [6,8] to study light propagation in the weak fiel limit for Schwarzschild (diagonal spacetime) and for a slowly rotating massive object (non-diagonal spacetime), respectively.

The equations of motion for photons can be obtained employing the so-called *null approximation*. It is known that the presence of an arbitrary medium in curved spacetimes makes photons move along bent trajectories (In contrast to flat spacetime in vacuum, where the photons' trajectories are straight lines). However, due to the assumption of a weak gravitational field, we can take into account only small deviations and use the components in flat spacetime of the photons' 4-momentum moving in a straight line along the z axis as an approximation (*the null approximation*). These components are given by [6,8]

$$p^{\alpha} = \left(\tfrac{\hbar\omega}{c}, 0, 0, \tfrac{n\hbar\omega}{c}\right) \quad \text{and} \quad p_{\alpha} = \left(-\tfrac{\hbar\omega}{c}, 0, 0, \tfrac{n\hbar\omega}{c}\right). \tag{10}$$

It is important to point out that both ω and n are evaluated at ∞ and we use the notation introduced in references [6,8] where

$$\omega = \omega(\infty) \quad \text{and} \quad n = n(\infty). \tag{11}$$

Hence, using Equations (6), (9) and (10) it is possible to compute the deflection angle for both diagonal and non-diagonal spacetimes. These angles will depend on the small perturbations h_{ij} and the plasma distribution.

Let's start with a diagonal spacetime. In this case, the non-zero components of metric tensor $g_{\alpha\beta}$ are those with $\alpha = \beta$. As a consequence, the function $W(x^{\alpha}, p_{\alpha})$ takes the form

$$W(x^{\alpha}, p_{\alpha}) = \frac{1}{2}\left[g^{00}p_0^2 + g^{lm}p_l p_m + \frac{\omega_e^2\hbar^2}{c^2}\right]. \tag{12}$$

Due to the null approximation, the 3-vector in the direction of the photon's momentum (first equation in Equation (6)) can be expressed as

$$p_i = \frac{n\hbar\omega}{c}e_i, \tag{13}$$

where $e_i = (0, 0, 1)$. Therefore, the second relation in Equation (6) becomes

$$\frac{de_i}{dz} = -\frac{1}{2}\frac{c^2}{n\hbar^2\omega^2}\left(g^{00}{}_{,i}(p_0)^2 + g^{lm}{}_{,i}p_l p_m + \frac{\hbar^2}{c^2}K_e N_{,i}\right) - e_i\frac{dn}{dz}.$$

According to reference [6], only the components of e_i that are perpendicular to the initial direction of propagation were taken into account. This means that the contribution to the deflection of photons is due only to the change in e_1 and e_2. Thus, after using the null approximation ($e_i = 0$) and the assumption of a weak gravitational field in Equation (1), the last equation reduces to

$$\tfrac{de_i}{dz} = \tfrac{1}{2}\left(h_{33,i} + \tfrac{1}{n^2}h_{00,i} - \tfrac{1}{n^2\omega^2}K_e N_{,i}\right), \quad i = 1, 2 \tag{14}$$

Equation (14) can be used to obtain the deflection angle, which is defined by [26–28]

$$\vec{\hat{\alpha}} = \mathbf{e}(+\infty) - \mathbf{e}(-\infty). \tag{15}$$

Thus, after integration, we obtain the following expression [6,8]

$$\hat{\alpha}_b = \frac{1}{2}\int_{-\infty}^{\infty}\frac{b}{r}\left(\frac{dh_{33}}{dr} + \frac{1}{1-\omega_e^2/\omega^2}\frac{dh_{00}}{dr} - \frac{K_e}{\omega^2-\omega_e^2}\frac{dN}{dr}\right). \tag{16}$$

Note that ω_e and n are evaluated at infinty and b is the impact parameter.

In a non-diagonal spacetime the components of the metric tensor $g_{\alpha\beta}$ do not vanish for $\alpha \neq \beta$. In this sense, the escalar function $W(x^\alpha, p_\alpha)$ takes the form [6,8]

$$W(x^\alpha, p_\alpha) = \frac{1}{2}\left[g^{00}p_0^2 + 2g^{0l}p_0p_l + g^{lm}p_lp_m + \frac{\omega_e^2\hbar^2}{c^2}\right]. \tag{17}$$

Note that Equation (17) differs from Equation (14) only in terms of the form $g^{0l}p_0p_l$. Thus, following the same process as in the case of a diagonal space-time, the second equation in Equation (4) becomes [6,8]

$$\frac{dp_i}{dz} = \frac{1}{2}\frac{n\hbar\omega}{c}\left(h_{33,i} + \frac{1}{n^2}h_{00,i} + \frac{1}{n}h_{03,i} - \frac{K_eN_{,i}}{n^2\omega^2}\right), \tag{18}$$

from which, after integration, the deflection angle for a non-diagonal spacetime in the presence of plasma is given by [6,8]

$$\hat{\alpha}_i = \frac{1}{2}\int_{-\infty}^{\infty}\left(h_{33,i} + \frac{\omega^2}{\omega^2-\omega_e^2}h_{00,i} + \frac{1}{n}h_{03,i} - \frac{K_eN_{,i}}{\omega^2-\omega_e^2}\right)dz\,. \tag{19}$$

3. Boosted Kerr Black Hole in the Presence of Plasma

The boosted Kerr black hole was obtained by I. D. Soares in 2017 [24]. This spacetime is a solution of Einstein's vacuum field equations which describe a boosted black hole relative to an asymptotic Lorentz frame. Nevertheless, in a recent paper by E. Gallo and T. Mädler [29] it is claimed that the boosted metric obtained by I. D. Soares can not be considered as a boosted Kerr black hole with respect to an asymptotically Lorentzian observer and, as the authors explain: *"care must be taken in the interpretation of the "boosted" Kerr metrics obtain by Soares."* [29]. For this reason, we consider important to point out that in this work (and in Ref. [30]) we have considered two approximations: a boosted Schwarzschild black hole with a boost velocity $v << 1$ and a slowly rotating boosted Kerr black hole. On the other hand, according to E. Gallo and T. Mädler: *"physical effects of a boosted rotating Kerr black hole do not differ at leading order from those of a boosted Schwarzschild black hole because for large values of the radial coordinate r, the effects of the spin enters at higher order of a $1/r^n$ expansion than those resulting from the mass"* [29]. Hence, our results agree with this observation since the deflection angle for a boosted Schwarchild black hole (with $v << 1$) has the same behavior as the slowly rotating black hole.

In the Kerr-Schild coordinates, the line element is given by

$$ds^2 = -\left(1 - \frac{2Mr}{\Sigma}\right)dt'^2 + \left(1 + \frac{2Mr}{\Sigma}\right)dr^2 + \frac{\Sigma}{\Lambda}d\theta^2 + \frac{A\sin^2(\theta)}{\Lambda^2\Sigma}d\phi^2$$

$$- \frac{4Mra\sin^2\theta}{\Lambda\Sigma}dt'd\phi - \frac{4Mr}{\Sigma}dt'dr - \frac{2a\sin^2\theta}{\Lambda}\left(1 - \frac{2Mr}{\Sigma}\right)drd\phi$$

with,

$$\Sigma = r^2 + a^2\left(\frac{\beta+\alpha\cos\theta}{\alpha+\beta\cos\theta}\right)^2, \quad \Lambda = (\alpha+\beta\cos\theta)^2, \quad A = \Sigma^2 + a^2(\Sigma + 2Mr)\sin^2\theta. \tag{20}$$

Note that the solution has three parameters: mass, rotation, and boots. Moreover, $a = J/M$ is the specific angular momentum of the compact object with total mass M, $\alpha = \cosh\gamma$, $\beta = \sinh\gamma$, and γ is the usual Lorentz factor which defines the boost velocity v by the formula $v = \tanh\gamma = \beta/\alpha$. The metric in (20) exactly reduces to Kerr when $\Lambda = 1$ ($v = 0$). Moreover, it is important to point out that the direction of the boost for the Kerr black hole is along the axis of rotation.

In this section, we compute the deflection angle for a boosted Kerr black hole in the presence of plasma using the weak field approximation discussed in Section 2. First, we consider the non-rotating case ($a = 0$) which correspond to the boosted Schwarzschild black hole, and then the slowly rotating case.

3.1. Non-Rotating Case

To study the behavior of $\hat{\alpha}$ in the presence of plasma for the non-rotating case, it is necessary to express the line element Equation (20) in Cartesian coordinates and find the small perturbations h_{ij}. Nevertheless, before doing so, we first consider the limit of $v << 1$. Hence, under this approximation, Equation (20) takes the form [30]

$$ds^2 = -\left(1-\frac{2M}{r}\right)dt'^2 + \left(1+\frac{2M}{r}\right)dr^2 + r^2(1-2v\cos\theta)d\theta^2 + r^2\sin^2\theta d\phi^2 - 4vr^2\sin^2\theta\cos\theta d\phi^2 - \frac{4M}{r}dt'dr.$$

Now, using the coordinate transformation

$$\bar{t} = t, \quad \bar{x} = r\sin\theta\cos\phi, \quad \bar{y} = r\sin\theta\sin\phi, \quad \bar{z} = r\cos\theta. \tag{21}$$

Equation (21) reduces to

$$ds^2 = ds_0^2 + h_{11}d\bar{x}^2 + h_{12}d\bar{x}d\bar{y} + h_{13}d\bar{x}d\bar{z} + h_{22}d\bar{y}^2 + h_{23}d\bar{y}d\bar{z} + h_{00}dt^2 + d\bar{z}^2h_{33}, \tag{22}$$

from which,

$$h_{00} = \tfrac{2M}{r} \quad \text{and} \quad h_{33} = \tfrac{2M}{r}\cos^2\theta - 2v\cos\theta\sin^2\theta. \tag{23}$$

The expressions for h_{11}, h_{12}, h_{13}, h_{22}, and h_{23} can be found in ref. [30]. Here $ds_0^2 = -dt^2 + d\bar{x}^2 + d\bar{y}^2 + d\bar{z}^2$. Now, after using Equation (16), the deflection angle in the non-ratating case is given by

$$\hat{\alpha}_b = \frac{2M}{b} + \frac{2Mb}{1-\frac{\omega_e^2}{\omega^2}}\int_0^\infty \frac{dz}{(b^2+z^2)^{\frac{3}{2}}} + \frac{bK_e}{2}\int_{-\infty}^{\infty}\frac{1}{\omega^2-\omega_e^2}\frac{1}{r}\frac{dN}{dr}dz. \tag{24}$$

From Equation (24) we note that, at first order, $\hat{\alpha}_b$ does not depend on the velocity. Hence, if we consider a uniform plasma (ω_e constant), and the approximation $1-n \ll \frac{\omega_e}{\omega}$, Equation (24) reduces to [6]

$$\hat{\alpha}_b = \frac{2M}{b}\left(1+\frac{1}{1-\frac{\omega_e^2}{\omega^2}}\right). \tag{25}$$

In Figure 2a we plotted $\hat{\alpha}_b$ as a function of ω_e^2/ω^2 for different values of $b/2M$. The plot shows that $\hat{\alpha}_b$ increases as the ration ω_e^2/ω^2 increases. On the other hand, for small values of $b/2M$ the values of the deflection angle are greater. For example, for $b/2M$ = 100 the figure shows that $\hat{\alpha}_b$ is greater than 0.2; however, for $b/2M$ = 50,100 the deflection angle is less than 0.1. It is also possible to see from the figure that $\hat{\alpha}_b$ has the value $4M/b$ when there is not plasma ($\omega_e = 0$).

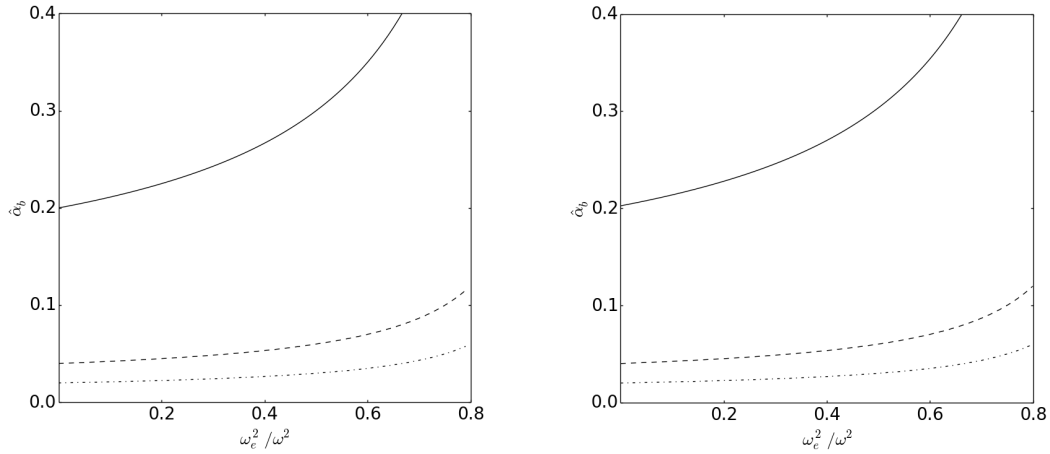

Figure 2. (**a**) Plot of $\hat{\alpha}_b$ vs. ω_e^2/ω^2 for $b/2M = 10$ (continuous line), $b/2M = 50$ (dashed line), and $b/2M = 100$ (dot-dashed line) for uniform plasma. (**b**) Plot of $\hat{\alpha}_b$ vs. ω_e^2/ω^2 for the rotating case. We used different values of the impact parameter: $b/2M = 10$ (continuous line), $b/2M = 50$ (dashed line), and $b/2M = 100$ (dot-dashed line). We assumed $\Lambda = 0.5$, $J_r/M^2 = 0.25$, $\sin\chi = 1$, and $\omega_e^2/\omega^2 = 0.5$. Note that there is a small increment for $b/2M = 10$ when we compare with Schwarzschild (left panel). Figures taken from Ref. [30].

3.2. Slowly Rotating Case

To study the behavior of the deflection angle in the slowly rotating case, we first express the line element in Equation (20) in the form [8,31]

$$ds^2 = -\left(1 - \frac{2M}{r}\right)dt^2 + \left(1 - \frac{2M}{r}\right)^{-1} dr^2 + r^2(d\theta^2 + \sin^2\theta d\phi^2) - 2\overline{\omega}_{LT} r^2 \sin^2\theta dt d\phi. \tag{26}$$

where $\overline{\omega}_{LT} = 2Ma/r^3 = 2\overline{J}/r^3$, with $\overline{J} = J/\Lambda$, is the Lense-Thirring angular velocity of the dragging of inertial frame. In this sense, due to the presence of non-diagonal terms in the line element (26), we use the form of $\hat{\alpha}$ obtained in Equation (19). Nevertheless, to obtain the small perturbation h_{ik}, we recall that the dragging effect on the inertial frame contributes to $\hat{\alpha}$ only utilizing the projection $\overline{J}_r$ of the angular momentum [8]. Thus, after the introduction of polar coordinates (b, χ) on the intersection point between the light ray and the xy-plane, where χ is the angle between $\vec{J}_r$ and $\vec{b}$, we find that [8] (see Figure 3)

$$h_{03} = -2\frac{\overline{J}_r b \sin\chi}{(b^2 + z^2)^{3/2}}. \tag{27}$$

Note that the deflection angle in Equation (19) will contain two contributions (In this manuscript we only consider de case in which $\chi = \pi/2$ so that $\hat{\alpha}_\chi = 0$). These contirbutions are given by [30] since h_{03} depends on b and χ

$$\begin{aligned} \hat{\alpha}_b &= \hat{\alpha}_{bS} - 2\overline{J}_r \sin\chi \int_0^\infty \left(\frac{1}{n(b^2 + z^2)^{3/2}} - \frac{3b^2}{n(b^2 + z^2)^{\frac{5}{2}}} \right) dz \\ \hat{\alpha}_\chi &= -2\overline{J}_r \cos\chi \int_0^\infty \frac{1}{n(b^2 + z^2)^{3/2}} dz, \end{aligned} \tag{28}$$

where $\hat{\alpha}_{bS}$ is the deflection angle for Schwarzschild given by Equation (24). Thus, for $\omega_e^2/\omega^2 \ll 1$, $\hat{\alpha}_b$ reduces to [30]

$$\hat{\alpha}_b = \underbrace{\frac{4M}{b}}_{\hat{\alpha}_{S1}} + \underbrace{\frac{2Mb}{\omega^2}\int_0^\infty \frac{\omega_e^2}{r^3}dz}_{\hat{\alpha}_{S2}} + \underbrace{\frac{bK_e}{\omega^2}\int_0^\infty \frac{1}{r}\frac{dN}{dr}dz}_{\hat{\alpha}_{S3}} + \underbrace{\frac{bK_e}{\omega^4}\int_0^\infty \frac{\omega_e^2}{r}\frac{dN}{dr}dz}_{\hat{\alpha}_{S4}}$$
$$+ \underbrace{\frac{2J_r}{\Lambda b^2}\sin\chi}_{\hat{\alpha}_{B1}} - \underbrace{\frac{J_r}{\Lambda\omega^2}\sin\chi\int_0^\infty \frac{\omega_e^2}{r^3}dz}_{\hat{\alpha}_{B2}} + \underbrace{\frac{3b^2J_r}{\Lambda\omega^2}\sin\chi\int_0^\infty \frac{\omega_e^2}{r^5}dz}_{\hat{\alpha}_{B3}}, \tag{29}$$

here $r = \sqrt{b^2 + z^2}$, and S and B stand for Schwarzschild and Boosted, respectively. Equation (29) is similar to that obtained by Kogan et. al in Ref. [6]: we also find the vacuum gravitational deflection $\hat{\alpha}_{S1}$, the correction to the gravitational deflection due to the presence of the plasma $\hat{\alpha}_{S2}$, the refraction deflection due to the inhomogeneity of the plasma $\hat{\alpha}_{S3}$, and its small correction $\hat{\alpha}_{S4}$. However, when the boosted Kerr metric is considered, three more terms appear: $\hat{\alpha}_{B1}$, $\hat{\alpha}_{B2}$, and $\hat{\alpha}_{B3}$. These are contributions due to the dragging of the inertial frame. The former is a constant that is presented in all distributions considered. The other two depend on plasma distribution.

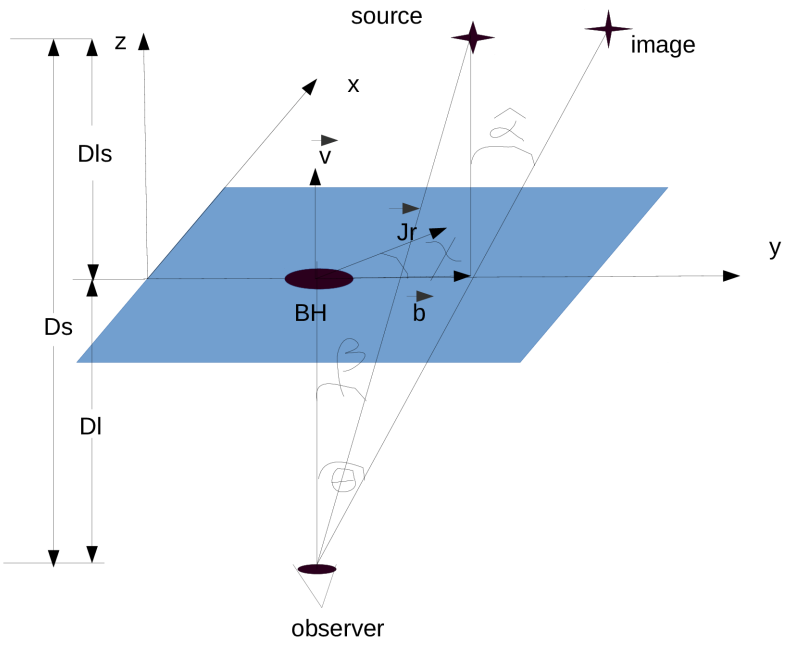

Figure 3. Schematic representation of the gravitational lensing system. Here, χ represents the inclination angle between the vectors $\mathbf{J}_r$ and $\mathbf{b}$. In the figure, D_s, D_l, and D_{ls} are the distances from the source to the observer, from the lens to the observer, and from the source to the lens, respectively. Figures taken from Ref. [30].

In the presence of uniform plasma, the deflection angle in Equation (29) takes the form

$$\hat{\alpha}_b = \underbrace{\frac{2M}{b}\left(1 + \frac{1}{1 - \frac{\omega_e^2}{\omega^2}}\right)}_{\hat{\alpha}_{bS}} + \underbrace{\frac{1}{\sqrt{1 - \frac{\omega_e^2}{\omega^2}}}\frac{2J_r}{b^2\Lambda}}_{\hat{\alpha}_{bD}}. \tag{30}$$

In Figure 4 left panel, we plot $\hat{\alpha}_{bS}$ and $\hat{\alpha}_b$ for the slowly rotating case as a function of the impact parameter $b/2M$. From the figure, we see that $\hat{\alpha}_b$ for a boosted Kerr black hole is greater than $\hat{\alpha}_{bS}$. This is due to the rotation and boosts velocity v, which is larger for small values of $b/2M$. On the other hand, for larger values of the impact parameter $b/2M$, this difference becomes very small, and both angles behave in the same way since $2J_r/(nb^2\Lambda) \to 0$ when $b/2M \to \infty$.

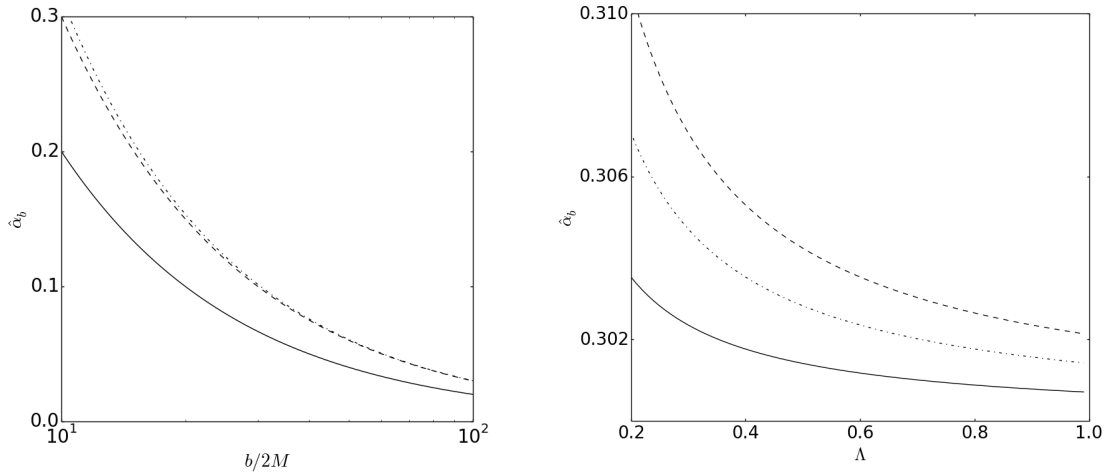

Figure 4. (**a**) Plot of $\hat{\alpha}_b$ vs. $b/2M$ in the presence of uniform plasma for the slowly rotating (dot-dashed line) and $\hat{\alpha}_{bS}$ (dashed line). In the figure it is also plotted the Schwarzschild case in vacuum (continuous line). We used $\Lambda = 0.5$, $J_r/M^2 = 0.25$, $\sin\chi = 1$, and $\omega_e^2/\omega^2 = 0.5$. (**b**) Plot of $\hat{\alpha}_b$ vs. Λ for $J_r/M^2 = 0.1$ (continuous line), $J_r/M^2 = 0.2$ (dot-dashed line) , and $J_r/M^2 = 0.3$ (dashed line). We assumed $b/2M = 10$, $\sin\chi = 1$, and $\omega_e^2/\omega^2 = 0.5$. Figures taken from Ref. [30].

On the other hand, in Figure 4 right panel, we plot Equation (30) as a function of Λ for different values of J_r. We took into account the condition in which $0 < \Lambda \leq 1$ in order to give the values. In this figure, for different values of Λ, we see that $\hat{\alpha}_b$ is bigger when $\Lambda \to 0$. Moreover, for $\Lambda = 1$, the deflection angle reduces to the value $\hat{\alpha}_{bS} + 2J_r/nb^2$.

Now, in order to study the behavior of $\hat{\alpha}$ in the presence of non-uniform plasma, it is necessary to know, according to Equation (30), the plasma concentration $N(r)$ and plasma frequency ω_e^2; both functions of the distribution density $\rho(r)$:

$$N(r) = \frac{\rho(r)}{\kappa m_p} \quad \text{and} \quad \omega_e^2 = K_e N(r) = \frac{K_e \rho(r)}{\kappa m_p}, \tag{31}$$

where m_p is the proton mass and κ is is a non-dimensional coeficient related to the dark matter contribution [6].

In the case of a singular isothermal sphere (**SIS**), the distribution density is given by

$$\rho(r) = \frac{\sigma_v^2}{2\pi r^2}, \tag{32}$$

where σ_v^2 is a one-dimensional velocity dispersion. The **SIS** model is often used in lens modeling of galaxies and clusters [32]. Hence, after using Equation (29), the deflection angle reduces to [30]

$$\hat{\alpha}_{SIS} = \frac{2}{\overline{b}} + \frac{1}{12\pi}\frac{\omega_c^2}{\omega^2 \overline{b}^3} - \frac{1}{16}\frac{\omega_c^2}{\omega^2 \overline{b}^2} + \frac{1}{2}\frac{\widetilde{J}_r}{\Lambda \overline{b}^2} - \frac{1}{48\pi}\frac{\widetilde{J}_r \omega_c^2}{\Lambda \omega^2 \overline{b}^4} + \frac{1}{20\pi}\frac{\widetilde{J}_r \omega_c^2}{\Lambda \omega^2 \overline{b}^4}, \tag{33}$$

where we define $\omega_c^2 = K_e \sigma_v^2 / M^2 \kappa m_p$, $\widetilde{J}_r = J_r/M^2$, and $\overline{b} = b/2M$.

In Figure 5 left panel, we show the plot of $\hat{\alpha}_{SIS}$ as a function of $\overline{b}$ for different values of Λ. According to the figure, there is no difference for values of $b/2M$ greater than 10. However, for $b/2M$ near to 10, there is a small difference. This means that $\hat{\alpha}_{SIS}$ is greater when Λ is small. When $\Lambda = 1$ ($v = 0$), we have the case of a slowly rotating massive object. In this sense, Λ has a small effect on the deflection angle. this behavior can be seen clearly in the right panel of Figure 5, where it is plotted $\hat{\alpha}_{SIS}$ as a function of Λ for different values of $\widetilde{J}_r$. Note that the boosted parameter is constrained to the interval $0 < \Lambda \leq 1$.

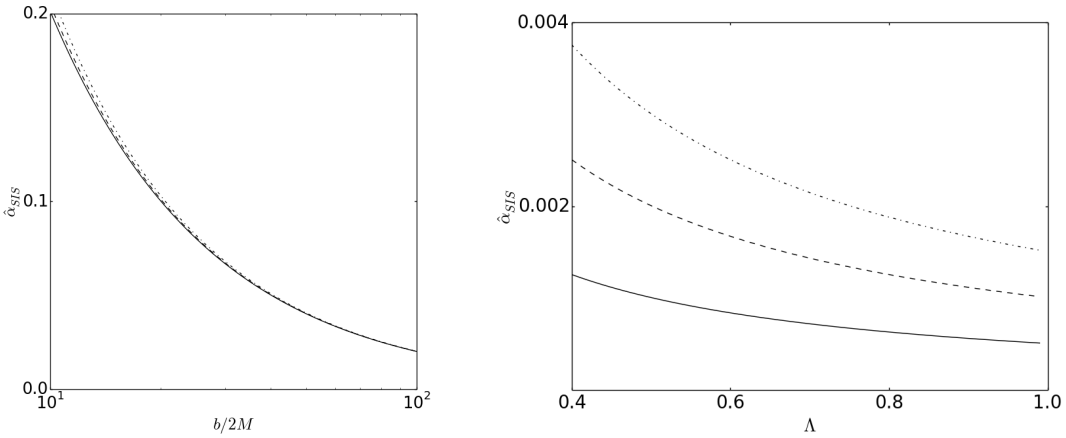

(**a**) (**b**)

Figure 5. (**a**) Plot of $\hat{\alpha}_{SIS}$ vs. $b/2M$ for $\Lambda = 1$ (continuous line), $\Lambda = 0.2$ (dashed line), and $\Lambda = 0.1$ (dot-dashed line). We used $J_r/M^2 = 0.25$, $\sin\chi = 1$, and $\omega_c^2/\omega^2 = 0.5$. (**b**) Plot of $\hat{\alpha}_{SIS}$ vs. Λ for $\widetilde{J}_r = 0.1$ (continuous line), $\widetilde{J}_r = 0.2$ (dashed line), and $\widetilde{J} = 0.3$ (dot-dashed line). We used, $\bar{b} = 10$, $\sin\chi = 1$, and $\omega_c^2/\omega^2 = 0.5$. Figures taken from Ref. [30]

The non-singular isothermal sphere (**NSIS**) is a model of plasma distribution where the singularity is replaced by a finite core. In this plasma, the density distribution is given by [33]

$$\rho(r) = \frac{\sigma_v^2}{2\pi(r^2+r_c^2)} = \frac{\rho_0}{\left(1+\frac{r^2}{r_c^2}\right)} \quad \text{with} \quad \rho_0 = \frac{\sigma_v^2}{2\pi r_c^2}. \tag{34}$$

Here r_c is the core radius. In the presence of a **NSIS**, the deflection angle in Equation (30) takes the form [30]

$$\begin{aligned}\hat{\alpha}_{NSIS} = {} & \frac{2}{\bar{b}} + \frac{2\bar{b}\omega_c^2}{\pi\omega^2}\left[\frac{1}{4\bar{b}^2\bar{r}_c^2} - \frac{\operatorname{arctanh}\left(\frac{\bar{r}_c}{\sqrt{4\bar{b}^2+\bar{r}_c^2}}\right)}{\bar{r}_c^3\sqrt{\bar{r}_c^2+4\bar{b}^2}}\right] - \frac{1}{2}\frac{\bar{b}\omega_c^2}{(4\bar{b}^2+\bar{r}_c^2)^{\frac{3}{2}}\omega^2} + \frac{2\widetilde{J}_r}{\Lambda\bar{b}^2} \\ & - \frac{\widetilde{J}_r\omega_c^2}{2\pi\Lambda\omega^2}\left[\frac{1}{4\bar{b}^2\bar{r}_c^2} - \frac{\operatorname{arctanh}\left(\frac{\bar{r}_c}{\sqrt{4\bar{b}^2+\bar{r}_c^2}}\right)}{\bar{r}_c^3\sqrt{\bar{r}_c^2+4\bar{b}^2}}\right] + \frac{6}{\pi}\frac{\bar{b}^2\widetilde{J}_r\omega_c^2}{\Lambda\omega^2}\left[\frac{2\bar{r}_c^2-12\bar{b}^2}{48\bar{b}^4\bar{r}_c^4} + \frac{\operatorname{arctanh}\left(\frac{\bar{r}_c}{\sqrt{4\bar{b}^2+\bar{r}_c^2}}\right)}{\bar{r}_c^5\sqrt{\bar{r}_c^2+4\bar{b}^2}}\right].\end{aligned} \tag{35}$$

In Figure 6 left panel, we show the behaviour of $\hat{\alpha}_{NSIS}$ as a function of $\bar{b}$ for different values of Λ. In the plot, since we are in the weak field limit, we consider $\bar{b} \gg \bar{r}_c$. The behavior is very similar to the singular plasma distribution: there are small differences in $\hat{\alpha}_{NSIS}$ when small values of Λ are considered, and no difference appears when the impact parameter $\bar{b}$ takes values greater than 10. Figure 6 right panel shows clearly this behavior.

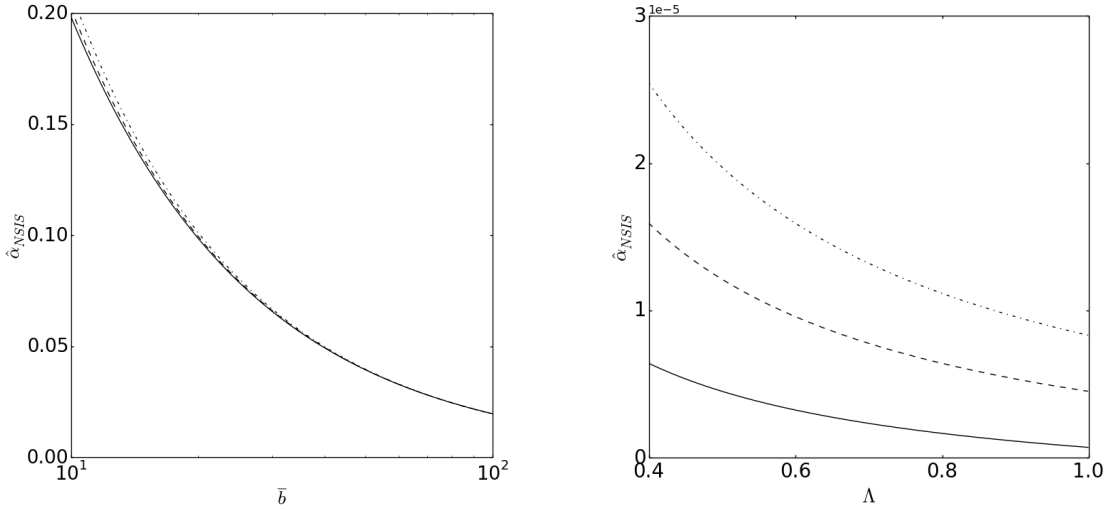

(**a**) (**b**)

Figure 6. (**a**) Plot of $\hat{\alpha}_{NSIS}$ vs. $\bar{b}$ for $\Lambda = 1$ (continuous line), $\Lambda = 0.25$ (dashed line), and $\Lambda = 0.1$ (dot-dashed line). We used, $\widetilde{J}_r = 0.25$, $\bar{r}_c = 10$, $\sin\chi = 1$, and $\omega_c^2/\omega^2 = 0.5$. (**b**) Plot of $\hat{\alpha}_{NSIS}$ vs. Λ for $\widetilde{J}_r = 0.1$ (continuous line), $\widetilde{J}_r = 0.2$ (dashed line), and $\widetilde{J} = 0.3$ (dot-dashed line). We used, $\bar{b} = 100$, $\bar{r}_c = 10$, $\sin\chi = 1$, and $\omega_c^2/\omega^2 = 0.5$. Note the scale used for the deflection angle: each value is multiplied by $1e-5 = 1\times10^{-5}$. Figures taken from Ref. [30].

Finally, we consider the deflection angle in the case of plasma in a galaxy cluster. Due to the large temperature of electrons in the cluster, the distribution can be considered as homogeneous. In this sense, it is possible to suppose a **SIS** distribution. Hence, the plasma density has the form [6]

$$\rho(r) = \rho_0\left(\frac{r}{r_0}\right)^{-s}, s = \frac{2\sigma_v^2}{\Re T}. \tag{36}$$

Therefore, after using Equation (29), the deflection angle has the form [30]

$$\begin{aligned}\hat{\alpha}_{PGC} = \frac{2}{\bar{b}} + \frac{\sqrt{\pi}}{2^{s+1}(s+1)}\frac{\bar{r}_0^s\omega_f^2}{\bar{b}^2\omega^2}\frac{\Gamma(\frac{s}{2}+1)}{\Gamma(\frac{s+1}{2})} - \frac{\sqrt{\pi}}{2^s}\frac{\omega_f^2}{\omega^2}\frac{\Gamma(\frac{s}{2}+1)}{\Gamma(\frac{s}{2})}\left(\frac{\bar{r}_0}{\bar{b}}\right)^s + \frac{2\widetilde{J}_r}{\Lambda\bar{b}^2} \\ - \frac{\pi}{2^{s+2}(s+1)}\frac{\widetilde{J}_r\bar{r}_0^2\omega_f^2}{\bar{b}^{s+2}\Lambda\omega^2}\frac{\Gamma(\frac{s}{2}+1)}{\Gamma(\frac{s+1}{2})} + \frac{3\sqrt{\pi}}{2^{s+2}(s+3)}\frac{\widetilde{J}_r\bar{r}_0^s\omega_f^2}{b^{s+2}\Lambda\omega^2}\frac{\Gamma(\frac{s+4}{2})}{\Gamma(\frac{s+1}{2})}.\end{aligned} \tag{37}$$

where we define $\omega_f^2 = \frac{K_e\rho_0}{\kappa m_p}$, $\bar{r}_0 = r_0/M$, $\widetilde{J}_r = J_r/M^2$, and $\bar{b} = b/2M$.

In Figure 7a,b we plot $\hat{\alpha}_{PGC}$ as a function of $\bar{b}$ and Λ, respectively. In In order to obtain these plots we considered the case $s << 1$ [6]. According to Figure 7, differences in the deflection angle can be seen clearly for the **PGC** distribution when compared with the previous distributions. Furthermore, Figure 7b shows that the deflection angle increases due to the dragging and small values of Λ. In Figure 7c, we show the behavior of $\hat{\alpha}$ as a function of the impact parameter $\bar{b}$ for all distributions. Observ that values of $\hat{\alpha}$ for the **PGC** distribution are grater than the other two distributions. In the figure, it is also possibel to see the small difference between **SIS** and **NSIS** distributions for small values of $b/2M$.

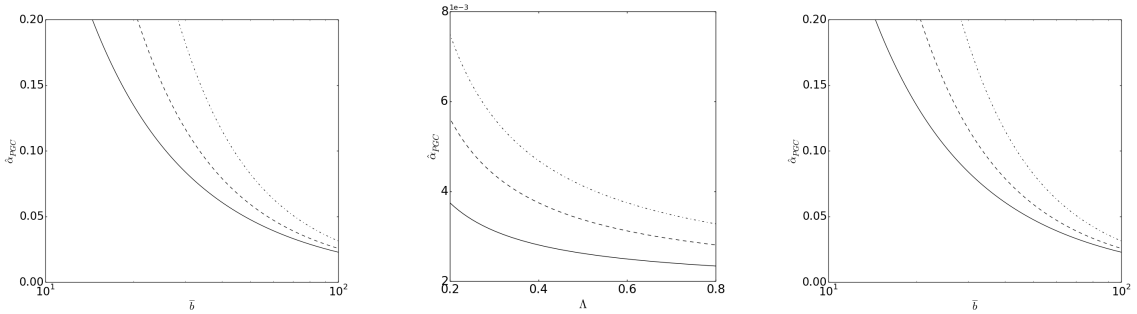

(**a**) (**b**) (**c**)

Figure 7. (**a**) Plot of $\hat{\alpha}_{PGC}$ vs. $\overline{b}$ for $\Lambda = 1$ (continuous line), $\Lambda = 0.25$ (dashed line), and $\Lambda = 0.1$ (dot-dashed line). We used, $\widetilde{J}_r = 0.25$, $\bar{r}_0 = 10$, $\sin\chi = 1$, $s = 0.03$, and $\omega_f^2/\omega^2 = 0.5$. (b) Plot of $\hat{\alpha}_{PGC}$ vs. Λ for $\widetilde{J}_r = 0.1$ (continuous line), $\widetilde{J}_r = 0.2$ (dashed line), and $\widetilde{J}_r = 0.3$ (dot-dashed line). We used $\bar{r}_0 = 10$, $\sin\chi = 1$, $s = 0.03$, $\overline{\mathbf{b}} = 100$ and $\omega_f^2/\omega^2 = 0.5$. Note the scale used for the deflection angle: each value is multiplied by $1e-3 = 1\times10^{-3}$. (**c**) Plot of $\hat{\alpha}$ vs. $\overline{b}$ for **SIS** (continuous line), **NSIS** (dashed line), and **PGC** (dot-dashed line). We used $\Lambda = 0.1$, $\bar{r}_c = 10$, $\bar{r}_0 = 10$, $\sin\chi = 1$, $s = 0.03$, and $\omega_f^2/\omega^2 = \omega_c^2/\omega^2 = 0.5$. For **NSIS** we use $\Lambda = 1$ since no difference from **SIS** was found. Figures taken from Ref. [30].

4. Lens Equation and Magnification in the Presence of Plasma

In this section, as an application, we study the magnification for a boosted Kerr black hole in the presence of plasma. In particular, we compare the uniform and singular isothermal distributions.

It is known that the lens equation relates the distance from the observer to the source Ds with the distance from the lens to the source D_{ls} and it is given by the relation [28]

$$\theta D_s = \beta D_s + \hat{\alpha} D_{ls}. \tag{38}$$

where $\hat{\alpha}$ is the deflection angle, and θ, β the image and source positions respectively (see Figure 8). According to Schneider et al., Equation (38) describes a general lensing situation in which the source is considered as a sphere $\mathbf{S}_S$ centered at O with radius D_s. Similarly, the deflector $\mathbf{S}_d$ is the sphere with radius D_l. The line connecting L, the observer O, and the point N is the "optical axis". Hence, If light rays were not affected by the gravitational field, S would have an undisturbed angular position β concerning this axis. Nevertheless, since gravity does affect light trajectories, the ray $SI'O$ from the source is deflected by an angle $\hat{\alpha}$ in such a way that an image is formed at position θ. Furthermore, since small values of angles are considered, It is to replace the ray $SI'O$ by its approximation SIO and the spheres $\mathbf{S}_S$ and $\mathbf{S}_d$ by their tangent planes [28], therefore, the situation looks like the one described in Figure 3.

On the other hand, due to the small values of the angles, the lensing effect is very small to be detected. Nevertheless, by considering the brightness of the source these effects can be seen because lensing changes the apparent brightness of the source. In this sense, to see these changes, the magnification can be considered. This quantity is defined as the ratio between the total brightness of all the images I_{tot} and the unlensed brightness of the source I_*. It is given by [8]

$$\mu_\Sigma = \frac{I_{tot}}{I_*} = \sum_k \left| \left(\frac{\theta_k}{\beta}\right) \left(\frac{d\theta_k}{d\beta}\right) \right|, \quad k = 1, 2, \ldots, m, \tag{39}$$

where m is the number of images, θ_k is the image position (the real roots of Equation (39)), and β is the angular position of the source (see Figure 3). According to Equation (39), to compute the magnification for different distributions, it is necessary to solve the lens equation (38). Thus, In the case of uniform plasma, Equation (38) reduces to [30]

$$\theta^3 - \beta\theta^2 - \frac{\theta_E^2}{2}\left(1 + \frac{1}{1-\frac{\omega_e^2}{\omega^2}}\right)\theta - \frac{\theta_E^2 \tilde{J}_r}{4\overline{D}_l \Lambda}\frac{1}{\sqrt{1-\frac{\omega_e^2}{\omega^2}}} = 0. \tag{40}$$

For the **SIS**, the lens equation takes the form [30]

$$\theta^3 - \beta\theta^2 - \frac{2D_{ls}}{D_l D_s}\theta - \frac{\overline{D}_{ls}}{\overline{D}_l^2 \overline{D}_s}\left(\frac{\tilde{J}_r}{2\Lambda} - \frac{\omega_c^2}{16\omega^2}\right) = 0. \tag{41}$$

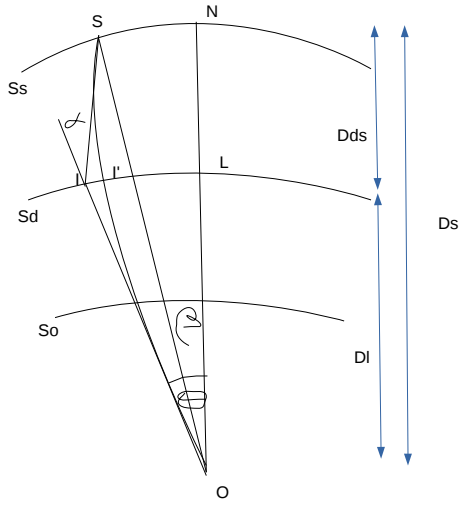

Figure 8. General lensing situation.

In both cases, we have considered small angles. This means that the impact parameter can be expressed as $b \approx D_l\theta$, with D_l denoting the distance from the observer to the lens. In addition, note that Equations (40) and (41) are cubic equations and it is possible to obtain three images (real roots). In Figure 9a,c, we plotted the behaviour of the total magnification as a function of the boosted parameter Λ for $\beta = 0.001$ and $\beta = 0.0001$ respectively. According to Figure 9a, when $\beta = 0.001$, the total magnification decreases as Λ increases. This means that $\mu_{\Sigma tot}$ decreases as the boosted velocity v of the black hole decreases. A similar behaviour can be seen from Figure 9c when $\beta = 0.0001$. Note that for small values of β, the magnitude of the total magnification increases. For example: when $\beta = 0.001$ the total magnification is about $\mu_{\Sigma tot} \approx 52.2$. However, when $\beta = 0.0001$, the value increases to $\mu_{\Sigma tot} \approx 522.2$.

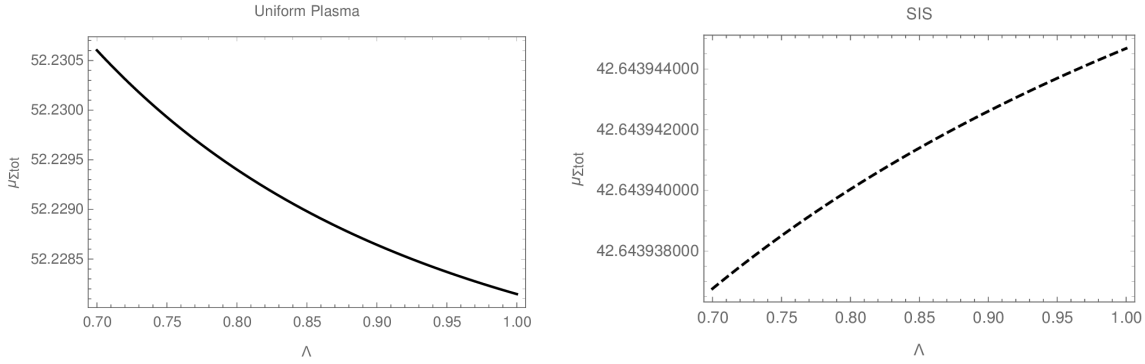

(**a**) (**b**)

Figure 9. *Cont*.

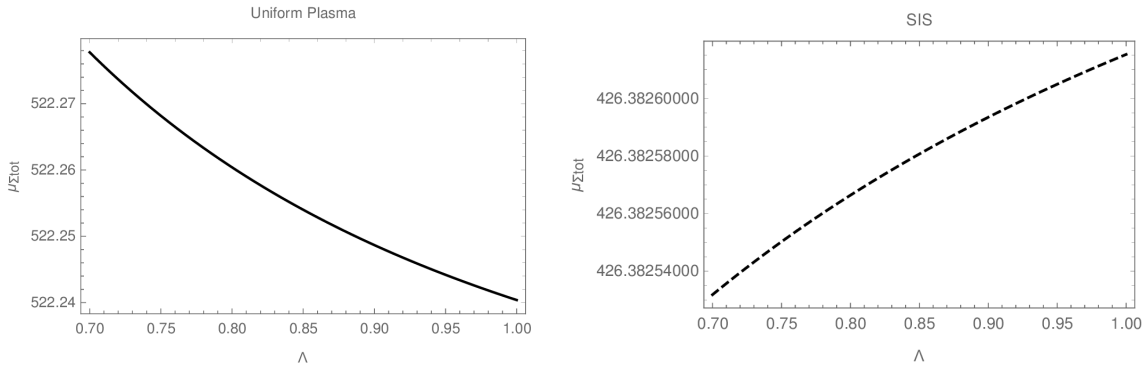

(**a**) (**b**)

Figure 9. (**a**) Plot of $\mu_{\Sigma tot}$ vs. Λ when $\beta = 0.001$ for uniform plasma. (**b**) Plot of $\mu_{\Sigma tot}$ vs. Λ when $\beta = 0.001$ for the **SIS** distribution. (**c**) Plot of $\mu_{\Sigma tot}$ vs. Λ when $\beta = 0.0001$ for unifomr plasma. (**d**) Plot of $\mu_{\Sigma tot}$ vs. Λ when $\beta = 0.0001$ for the **SIS** distribution. In all the figures we considered $\overline{D}_{ls} = 10$, $\overline{D}_l = 100$, $\overline{D}_s = 110$, $\omega_e^2/\omega^2 = \omega_c^2/\omega^2 = 0.5$, $\theta_E = 0.001818$, and $\tilde{J}_r = 0.3$. Figures taken from Ref. [30].

On the other hand, In Figure 9b,d, we plotted the behaviour of $\mu_{\Sigma tot}$ as a function of the boosted parameter Λ for $\beta = 0.001$ and $\beta = 0.0001$ respectively. In contrast to uniform plasma, the total magnification increases as Λ increases. Moreover, for small values of β, $\mu_{\Sigma tot}$ increases. Finally, in Figure 10 we show the behaviour of $\mu_{\Sigma tot}$ as a function of the boosted parameter Λ for uniform plasma and **SIS** distributions. Note that the behaviour of $\mu_{\Sigma tot}$ in the **SIS** distribution is not symmetric.

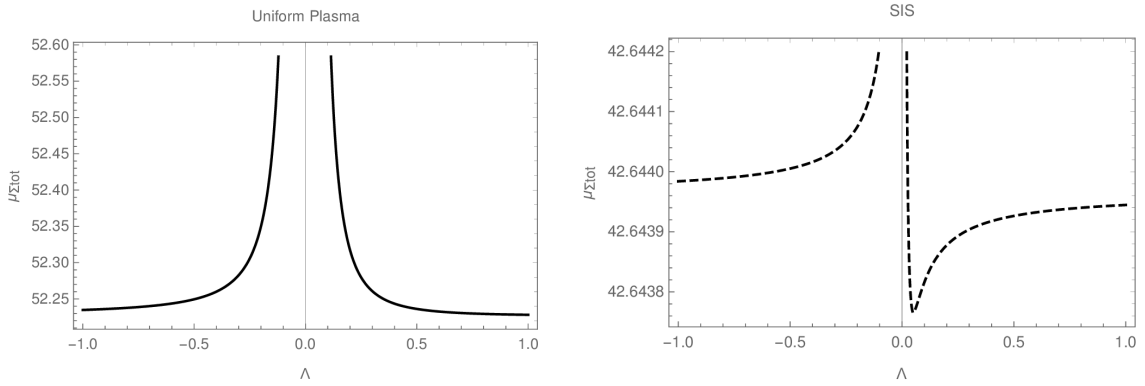

(**a**) (**b**)

Figure 10. (**a**) Plot of $\mu_{\Sigma tot}$ vs. Λ when $\beta = 0.001$ for uniform plasma. (**b**) Plot of $\mu_{\Sigma tot}$ vs. Λ when $\beta = 0.001$ for the **SIS** distribution. In all the figures we considered $\overline{D}_{ls} = 10$, $\overline{D}_l = 100$, $\overline{D}_s = 110$, $\omega_e^2/\omega^2 = \omega_c^2/\omega^2 = 0.5$, $\theta_E = 0.001818$, and $\tilde{J}_r = 0.3$. Figures taken from Ref. [30].

5. Conclusions

In this work we studied the deflection angle for a boosted Kerr metric in the presence of both uniform and non-uniform plasma distributions (where three different cases were considered). First we studied the deflection angle for the non-rotating case in the presence of uniform plasma ($\omega_e =$ costant) by considering small values of v. We found that $\hat{\alpha}_b$ does not dependent, at first order, on the velocity v. It was also found that, after the approximation $1 - n \ll \frac{\omega_e}{\omega}$, the deflection angle reduces to the same expression obtained in Ref. [6] (see Equation (25)). In the case of the slowly rotating case, the deflection angle $\hat{\alpha}_b$ in Equation (30) contains two terms: the Schwarzschild angle $\hat{\alpha}_{bS}$, and the contribution due to the dragging $\hat{\alpha}_{bD}$. This result is quite similar to that of V.S Morozova et al. However, in contrast with their result, Equation (30) also depends on the parameter Λ. Therefore, $\hat{\alpha}$ depends on v only when the dragging takes place.

In the presence of non-uniform plasma, we consider the deflection angle as a function of $\bar{b}$ and Λ for different distributions. We found that $\hat{\alpha}$ is affected by the presence of plasma and is greater when compared with vacuum and uniform distributions. Moreover, we found again that $\hat{\alpha}$ increases not only due to the dragging, but also when small values of the boosted parameter Λ are considered. In this work, we also found two important constraints. In the case of **NSIS**, r_c must have values greater than $6M$. If the core radius r_c is smaller than this limit the deflection angle becomes negative at some point and will not agree with the usual behavior when $b \to \infty$ [30]. On the other hand, regarding the **PGC**, we found that s must be different from -1 or -3 as can be seen from Equation (37). Nevertheless, this condition is fulfilled since we consider positive values of $s << 1$.

Finally, we compare the total magnification for uniform and **SIS** plasma distributions. According to Figure 9, for small values of v ($0.7 \leq \Lambda \leq 1$), the total magnification is greater in the case of homogeneous plasma. Furthermore, it is important to point out that the total magnification has small changes in both distributions. In the case of uniform plasma $\mu_{\Sigma tot}$ ranges from 52.2285 to 52.2305, and from 42.643938 to 42.643944 in the **SIS**. On the other hand, when we compare both models, we see that the behavior of $\mu_{\Sigma tot}$ is different. When the boosted Kerr black hole moves towards ($\Lambda > 0$) or away ($\Lambda < 0$) from the observer the behavior is very similar (there is a small difference when $\Lambda \to -1$ and $\Lambda \to 1$). However, when we consider the **SIS** distribution, the behavior is not symmetric. In both cases, this behavior is due to cinematic effects.

Author Contributions: A.-A. gave the idea of the project. C.A.B.-G. work on the calculations. Both authors work on the preparation of the manuscript.

Funding: This research received no external funding.

Acknowledgments: C.A.B.-G. acknowledges support from the China Scholarship Council (CSC), grant No. 2017GXZ019022. A.-A acknowledges support from Grant No. VA-FA-F-2-008 and No. YFA-Ftech-2018-8 of the Uzbekistan Ministryfor Innovation Development, by the Abdus Salam International Centre for Theoretical Physics through Grant No. OEA-NT-01 and by Erasmus+ exchange grant between Silesian University in Opava and National University of Uzbekistan.

Conflicts of Interest: The authors declare no conflicts of interest.

Abbreviations

The following abbreviations are used in this manuscript:

SIS	Singular Isothermal Sphere
NSIS	Non-Singular Isothermal Sphere
PGC	Plasma in a Galaxy Cluster

References

1. Abbott, B.P.; Abbott, R.; Abbott, T.D.; Abernathy, M.R.; Acernese, F.; Ackley, K.; Adams, C.; Adams, T.; Addesso, P.; Adhikari, R.X.; et al. Tests of general relativity with GW150914. *arXiv* **2016**, arXiv:1602.03841.
2. Abbott, B.P.; Abbott, R.; Abbott, T.D.; Abernathy, M.R.; Acernese, F.; Ackley, K.; Adams, C.; Adams, T.; Addesso, P.; Adhikari, R.X.; et al. Properties of the Binary Black Hole Merger GW150914. *arXiv* **2016**, arXiv:1602.03840.
3. Morozova, V.S.; Rezzolla, L.; Ahmedov, B.J. Nonsingular electrodynamics of a rotating black hole moving in an asymptotically uniform magnetic test field. *Phys. Rev. D* **2014**, *89*, 104030.
4. Lyutikov, M. Schwarzschild black holes as unipolar inductors: Expected electromagnetic power of a merger. *Phys. Rev. D* **2011**, *83*, 064001.
5. Synge, J.L. *Relativity: The General Theory*; North-Holland: Amsterdam, The Netherlands, 1960.
6. Bisnovatyi-Kogan, G.S.; Tsupko, O.Y. Gravitational lensing in a non-uniform plasma. *Mon. Not. R. Astron. Soc.* **2010**, *404*, 1790–1800.
7. Tsupko, O.Y.; Bisnovatyi-Kogan, G.S. On gravitational lensing in the presence of a plasma. *Gravit. Cosmol.* **2012**, *18*, 117–121.

8. Morozova, V.S.; Ahmedov, B.J.; Tursunov, A.A. Gravitational lensing in a non-uniform plasma. *Mon. Not. R. Astron. Soc.* **2013**, *346*, 513–520.
9. Rogers, A. Gravitational Lensing of Rays through the Levitating Atmospheres of Compact Objects. *Universe* **2017**, *3*, 3.
10. Rogers, A. Escape and Trapping of Low-Frequency Gravitationally Lensed Rays by Compact Objects within Plasma. *Mon. Not. R. Astron. Soc.* **2017**, *465*, 2151–2159
11. Kichenassamy, S.; Krikorian, R.A. Relativistic radiation transport in dispersive media. *Phys. Rev. D* **1985**, *32*, 1866.
12. Perlick, V.; Tsupko, O.Y. Light propagation in a plasma on Kerr spacetime: Separation of the Hamilton-Jacobi equation and calculation of the shadow. *Phys. Rev. D* **2017**, *95*, 104003.
13. Perlick, V.; Tsupko, O.Y.; Bisnovatyi-Kogan, G.S. Influence of a plasma on the shadow of a spherically symmetric black hole. *Phys. Rev. D* **2015**, *92*, 104031.
14. de Vries, A. The apparent shape of a rotating charged black hole, closed photon orbits and the bifurcation set A_4. *Class. Quantum Gravity* **1999**, *17*, 123–144.
15. Abdujabbarov, A.; Ahmedov, B.; Dadhich, N.; Atamurotov, F. Optical properties of a braneworld black hole: Gravitational lensing and retrolensing. *Phys. Rev. D* **2017**, *96*, 084017, doi:10.1103/PhysRevD.96.084017.
16. Abdujabbarov, A.; Amir, M.; Ahmedov, B.; Ghosh, S.G. Shadow of rotating regular black holes. *Phys. Rev. D* **2016**, *93*, 104004, doi:10.1103/PhysRevD.93.104004.
17. Abdujabbarov, A.A.; Rezzolla, L.; Ahmedov, B.J. A coordinate-independent characterization of a black hole shadow. *Mon. Not. Roy. Astron. Soc.* **2015**, *454*, 2423–2435, doi:10.1093/mnras/stv2079.
18. Abdujabbarov, A.; Toshmatov, B.; Stuchlík, Z.; Ahmedov, B. Shadow of the rotating black hole with quintessential energy in the presence of plasma. *Int. J. Mod. Phys. D* **2016**, *26*, 1750051, doi:10.1142/S0218271817500511.
19. Bambi, C.; Freese, K. Apparent shape of super-spinning black holes. *Phys. Rev. D* **2009**, *79*, 043002, doi:10.1103/PhysRevD.79.043002.
20. Bambi, C.; Yoshida, N. Shape and position of the shadow in the $\delta = 2$ Tomimatsu-Sato space-time. *Class. Quant. Grav.* **2010**, *27*, 205006, doi:10.1088/0264-9381/27/20/205006.
21. Turimov, B.; Ahmedov, B.; Abdujabbarov, A.; Bambi, C. Gravitational lensing by magnetized compact object in the presence of plasma. *arXiv* **2018**, arXiv:1802.03293.
22. Ahmedov, B.; Turimov, B.; Stuchlík, Z.; Tursunov, A. Optical properties of magnetized black hole in plasma. *Int. J. Mod. Phys. Conf. Ser.* **2019**, *49*, 1960018, doi:10.1142/S2010194519600188.
23. Li, Z.; Bambi, C. Measuring the Kerr spin parameter of regular black holes from their shadow. *J. Cosmol. Astropart. Phys.* **2014**, *1401*, 041, doi:10.1088/1475-7516/2014/01/041.
24. Soares, I.D. A boosted Kerr black hole solution and the structure of a general astrophysical black hole. *Gen. Rel. Grav.* **2017**, *49*, 77.
25. Wald, R.M. *General Relativity*; Chicago University Press: Chicago, IL, USA, 1984; doi:10.7208/chicago/9780226870373.001.0001.
26. Perlick, V. *Ray Optics, Fermat's Principle, and Applications to General Relativity*; Springer: Berlin, Germany, 2000.
27. Perlick, V. Gravitational lensing from a spacetime perspective. *Living Rev. Rel.* **2004**, *7*, 9.
28. Schneider, P.; Ehlers, J.; Falco, E.E. *Gravitational Lenses*; Springer: Cham, Switzerland, 1999; ISSN 0941-7834.
29. Gallo, E.; Mädler, T. Comment on "Boosted Kerr black holes in general relativity". *arXiv* **2019**, arXiv:1906.08761.
30. Benavides-Gallego, C.A.; Abdujabbarov, A.A.; Bambi, C. Gravitational lensing for a boosted Kerr black hole in the presence of plasma. *Eur. Phys. J. C* **2018**, *78*, 694, doi:10.1140/epjc/s10052-018-6170-9.
31. Hartle, J.B.; Thorne, K.S. Slowly Rotating Relativistic Stars. II. Models for Neutron Stars and Supermassive Stars. *Astrophys. J.* **1968**, *153*, 807, doi:10.1086/149707.
32. Chandrasekhar, S. *An Introduction to the Study of Stellar Structure*; Dover Publications: New Haven, CT, USA, 1939.
33. Hinshaw, G.; Krauss, L.M. Gravitational lensing by isothermal spheres with finite core radii-Galaxies and dark matter. *Astrophys. J.* **1987**, *320*, 468–476, doi:10.1086/165564.